



Comparison of single-postlabeling delay and seven-delay three-dimensional pseudo-continuous arterial spin labeling in the assessment of intracranial atherosclerotic disease

Hongwei Yu¹, Yiping Ouyang², Yibo Feng³, Shilong Sun¹, Linwei Zhang⁴, Zunjing Liu⁴, Hong Tian⁵, Sheng Xie¹

¹Department of Radiology, China-Japan Friendship Hospital, Beijing, China; ²China Medical University-The Queen's University of Belfast Joint College, China Medical University, Shenyang, China; ³Department of Ultrasound Medicine, China-Japan Friendship Hospital, Beijing, China; ⁴Department of Neurology, China-Japan Friendship Hospital, Beijing, China; ⁵Department of Neurosurgery, China-Japan Friendship Hospital, Beijing, China

Contributions: (I) Conception and design: S Xie, H Yu; (II) Administrative support: S Xie; (III) Provision of study materials or patients: L Zhang, Z Liu, H Tian; (IV) Collection and assembly of data: Y Feng, S Sun; (V) Data analysis and interpretation: Y Ouyang; (VI) Manuscript writing: All authors; (VII) Final approval of manuscript: All authors.

Correspondence to: Sheng Xie. Department of Radiology, China-Japan Friendship Hospital, No. 2 East Yinghua Road, Chaoyang District, Beijing 100029, China. Email: xs_mri@126.com.

Background: The assessment of cerebral blood flow (CBF) is crucial in the evaluation of intracranial atherosclerotic disease. This study was performed to compare single postlabeling delay (PLD) 3-dimensional pseudo-continuous arterial spin labeling (3D-pCASL) and 7-delay 3D-pCASL magnetic resonance imaging in patients with intracranial atherosclerotic stenosis.

Methods: A total of 26 patients with moderate to severe atherosclerotic stenosis or occlusion of an intracranial artery were prospectively enrolled in the study. Perfusion parameters were obtained in various regions of interest (ROIs), namely CBF for single PLDs of 1,525 ms ($CBF_{1525\text{ ms}}$), 2,025 ms ($CBF_{2025\text{ ms}}$), and 2,525 ms ($CBF_{2525\text{ ms}}$) with 3D-pCASL, as well as arterial transit time (ATT) and transit-corrected CBF ($CBF_{\text{transit-corrected}}$) for 7-delay 3D-pCASL. The consistency of the perfusion parameters between single-PLD 3D-pCASL and 7-delay 3D-pCASL was investigated, and the relationship between vascular stenosis and perfusion parameters was explored.

Results: Bland-Altman plots compared the CBF values derived from single-PLD 3D-pCASL to those from $CBF_{\text{transit-corrected}}$. ATT significantly correlated with the difference between $CBF_{\text{transit-corrected}}$ and $CBF_{1525\text{ ms}}$, $CBF_{2025\text{ ms}}$, and $CBF_{2525\text{ ms}}$, respectively ($P < 0.05$). Binary logistic regression analysis revealed that the $CBF_{\text{transit-corrected}}$ and ATT correlated with the presence of moderate or more severe stenotic vascular territories ($P < 0.05$).

Conclusions: The single-PLD 3D-pCASL and the 7-delay 3D-pCASL showed inconsistencies in the assessment of CBF, and the perfusion parameters generated under the standard single-PLD 3D-pCASL were more affected by ATT. Moreover, $CBF_{\text{transit-corrected}}$ and ATT were consistent with stenotic vascular territories, which is useful in the evaluation of intracranial atherosclerotic disease.

Keywords: Magnetic resonance imaging (MRI); arterial spin labeling; arterial transit time (ATT); intracranial atherosclerotic stenosis (ICAS); hemodynamics

Submitted Sep 15, 2022. Accepted for publication Jan 29, 2023; Published online Feb 09, 2023.

doi: 10.21037/qims-22-969

View this article at: <https://dx.doi.org/10.21037/qims-22-969>

Introduction

Acute ischemic stroke secondary to intracranial large-vessel thromboembolic stenosis or occlusion has substantial morbidity and mortality (1). Intracranial atherosclerotic stenosis (ICAS) causes hemodynamic disorders and thromboembolic events, leading to reduced cerebral blood perfusion. The severity of ischemia is essential for determining treatment strategies and making prognostic judgments. Currently, arterial spin labeling (ASL) is performed using various sequences, such as continuous arterial spin labeling (CASL) (2), pulsed arterial spin labeling (PASL) (3), and pulsed continuous arterial spin labeling (pCASL), to acquire measurements of cerebral blood flow (CBF) (4). The pCASL technology uses single postlabeling delay (PLD) to generate CBF and has been reported to be reliable in normal controls. Thus, it has become more widely used and accepted. However, a previous study demonstrated that the best delay time after labeling for healthy people is 1,800 ms, and the PLD should be increased for middle-aged and older adults (5). The selection of a short PLD may result in a false underestimation of the CBF (6). Therefore, uncertainty regarding the arterial transit time (ATT) in intracranial atherosclerotic disease may affect the evaluation of hemodynamic status (7).

Under the Hadamard encoding scheme, multidelay pCASL produces ASL images with several PLD times and achieves quantification of both CBF and ATT (8,9). Multiple PLDs may improve the accuracy of CBF quantification, as well as offer additional hemodynamic measures (10). Several studies have reported high reliability and reproducibility in clinical applications (11,12). For example, Wang *et al.* demonstrated that the correlation between ASL CBF and computed tomography (CT) perfusion was improved using the multidelay pCASL protocol compared to CBF acquired at a single PLD of 2 s in patients with Moyamoya disease (13). Fan *et al.* also reported no difference between multidelay ASL and positron emission tomography (PET) in the detection of abnormal perfusion, but standard ASL overestimated the degree of patients' hypoperfusion (14). However, it is not practical to improve the spatial resolution of multidelay pCASL due to the longer imaging time required. Moreover, multidelay pCASL is not yet widely available in clinical centers. Some researchers have designed studies using single-PLD pCASL following the consensus recommendation for clinical ASL (15,16). It has also been suggested that in patients with known cerebrovascular

disease, alternative ASL imaging strategies could be considered, including long-label, long-PLD using single-time-point ASL and multidelay ASL (17). However, the consistency of single PLD and multidelay pCASL in the quantification of CBF remains unclear in cerebrovascular disease. In a previous study conducted in patients with Moyamoya disease, long-label, long-delay ASL obtained reliable CBF estimates comparable to the gold-standard PET, which was superior to standard-delay and multidelay ASL (18). In order to determine the clinical feasibility of pCASL in patients with cerebrovascular disease and variable ATTs, we compared the difference between the CBF measurements of single-PLD 3-dimensional (3D)-pCASL and 7-delay 3D-pCASL in intracranial large-vessel thromboembolic stenosis or occlusion caused by atherosclerosis and investigated the relationship between vascular lesions and CBF in the corresponding regions.

Methods

Ethical statement

The study was conducted in accordance with the Declaration of Helsinki (as revised in 2013). The study protocol was approved by the Institutional Review Board of the China-Japan Friendship Hospital (No. 2015-23). Informed consent was obtained from each patient.

Study population

A total of 26 patients [18 men, 8 women; mean age \pm standard deviation: 67.3 \pm 10.3 years] were prospectively enrolled at the Radiology Department of the China-Japan Friendship Hospital from January to December 2021. The inclusion criteria were as follows: (I) diagnosis of moderate to severe intracranial artery stenosis or occlusion with computed tomography angiography (CTA) and magnetic resonance angiography (MRA); (II) with symptoms of ischemic cerebrovascular disease; and (III) presence of risk factors for atherosclerosis. The exclusion criteria were the following: (I) presence of diseases that could affect intracranial hemodynamics, such as intracranial space-occupying lesions, arteriovenous fistula, cerebral edema, and massive cerebral infarction; (II) history of cerebral hemorrhage and brain surgery; (III) extracranial carotid artery and vertebral artery (VA) stenosis \geq 50% or occlusion detected with head and neck CTA; (IV) presence of systemic diseases that could affect cerebral blood flow, such as serious

cardiovascular disease, severe anemia, and hypovolemia; (V) intake of medications that could markedly affect brain blood flow; and (VI) presence of MRI contraindications, such as metal implantation, pacemaker implantation, and claustrophobia.

MRI data acquisition

A 3.0-T magnetic resonance imaging scanner (Discovery MR750, GE Healthcare, IL, Chicago, USA) with an 8-channel head coil was used for imaging. The MRI sequences included T1-weighted imaging, T2-weighted imaging, diffusion-weighted imaging, 3D time-of-flight MRA, single-PLD 3D-pCASL, and 7-delay 3D-pCASL sequences. The sequence of the single-PLD 3D-pCASL was acquired using 3D spiral acquisition (1,024×8 arms) with a labeling duration of 1.5 s and PLDs of 1,525, 2,025, and 2,525 ms. The average number of signals was 3, and the scan times were 4 min 36 s, 4 min 48 s, and 5 min 16 s for the single-PLD 3D-pCASL. The key scanning parameters were as follows: field of view (FOV) 24 cm × 24 cm, echo time 14.6 ms, bandwidth 62.5 kHz, slice thickness 4 mm, number of slices 32, and spatial resolution 2.46 mm × 2.46 mm × 4 mm. The 7-delay 3D-pCASL images were acquired at the following 7 consecutive labeling time points: 0.22, 0.26, 0.30, 0.37, 0.48, 0.68, and 1.18 s, with labeling durations of 4 s and PLDs of 1.00, 1.22, 1.48, 1.78, 2.15, 2.62, and 3.32 s. The prescription of locations was the same as that of the single-PLD 3D-pCASL sequences, with a resolution of 4.76 mm × 4.76 mm × 4 mm. The number of excitations was 1, and the scanning time for the 7-delay pCASL was 3 min 38 s. Images were reconstructed using the Interactive Data Language (IDL)-based RWCON code and then stored in the database as Digital Imaging and Communications in Medicine (DICOM) images.

MRI data processing

A GE ADW 4.5 workstation (GE Healthcare) with FuncTool v. 9.4 (GE Healthcare) software was used for single-PLD 3D-pCASL and 7-delay 3D-pCASL raw data postprocessing. Perfusion parameter maps of CBF were obtained for single-PLD 3D-pCASL at 3 different PLD times, namely 1,525 ms (CBF_{1525 ms}), 2,025 ms (CBF_{2025 ms}), and 2,525 ms (CBF_{2525 ms}). Perfusion images were corrected for motion, and perfusion difference images were generated by pairwise subtraction between time-matched label and control images, which was followed by averaging to generate the mean difference

images. To determine ASL-derived CBF mapping, the following flow calculation formula was applied (19):

$$f = \frac{\lambda (S_{\text{ctrl}} - S_{\text{lbl}}) \left(1 - e^{-\frac{\omega}{T_{1g}}}\right)}{2\alpha T_{1b} \left(1 - e^{-\frac{\tau}{T_{1b}}}\right)} S_{\text{ref}} e^{\frac{\omega}{T_{1b}}} \quad [1]$$

where f is the flow, multiplied by a scaling factor (6,000,000) and converted to physiological units of mL/100 mL gray matter/min; S is the acquired signal on control (ctrl), labeled (lbl) signal, or the reference image; T_{1b} and T_{1g} are the T1 values of blood and gray matter (1.6 and 1.2 s, respectively); α is the labeling efficiency, assumed to be 0.8; λ is the cortex-blood partition coefficient value (0.9); and, τ and ω represent labeling duration (1,500 ms) and PLD time (e.g. 1,525 ms), respectively.

For the 7-delay 3D-pCASL, ATT and CBF corrected with ATT (CBF_{transit-corrected}) maps were generated. The transit time map is estimated with the signal-weighted delay method described by Dai *et al.* (20). CBF_{transit-corrected} maps were calculated through incorporating the combined delay image and transit delay (δ), as follows:

$$CBF = \frac{6000e^{\delta/T_{1a}}}{2\epsilon T_{1a} \left(e^{-\max(PLD-\delta,0)/T_{1a}} - e^{-\max(LD+PLD-\delta,0)/T_{1a}} \right)} \frac{P}{S_r} \quad [2]$$

where CBF is CBF in mL/100 g/min; PLD reflects the shortest PLD (1.0 s); LD is the entire labeling duration (4.0 s); T_{1a} and T_{1t} are the longitudinal relaxation of arterial blood (1.6 s) and gray matter (1.2 s), respectively; ϵ is the combined efficiency of labeling and background suppression (0.63); P represents the signal intensity in the perfusion-weighted image; and R is the signal intensity of the reference image. The reference image is scaled by $s_r = \lambda(1 - e^{-2/T_{1.2}})$ to account for the combined effect of the blood-brain partition coefficient ($\lambda=0.9$).

Circular regions of interest (ROIs) of about 300–400 mm² were manually prescribed in the bilateral frontal lobes, parietal lobes, temporal lobes, occipital lobes, cerebellum, and basal ganglia (Figures 1–3) on these maps with a copy-and-paste approach being used to ensure that the locations and areas were exactly the same.

A senior radiologist with more than 20 years' experience in neuroradiology and a radiologist with 10 years' experience evaluated the CTA and MRA images. The

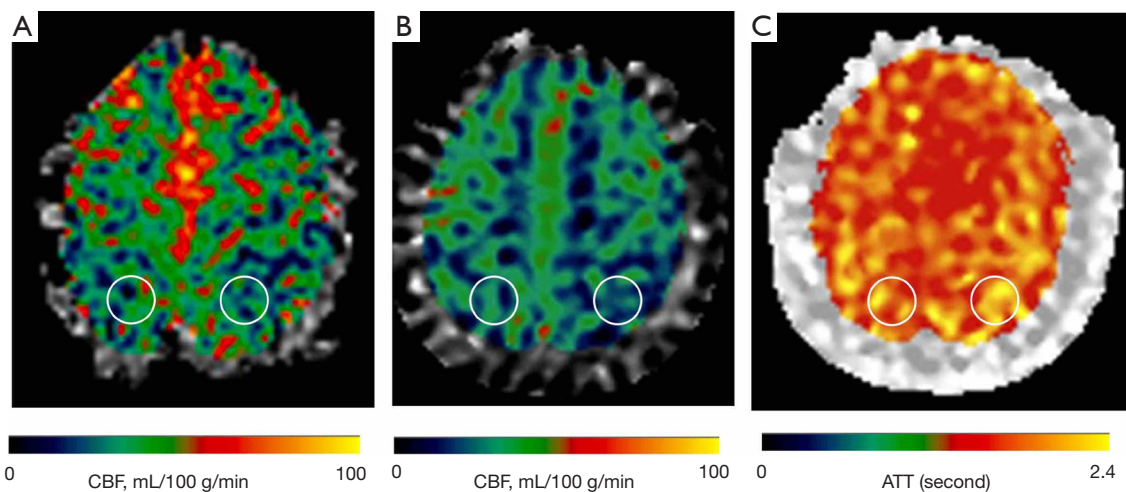


Figure 1 ROIs of the bilateral parietal lobes. (A) PLD =1,525 ms cerebral blood flow map. (B) Transit-corrected cerebral blood flow map. (C) ATT map. ATT, arterial transit time; CBF, cerebral blood flow; ROI, region of interest; PLD, postlabeling delay.

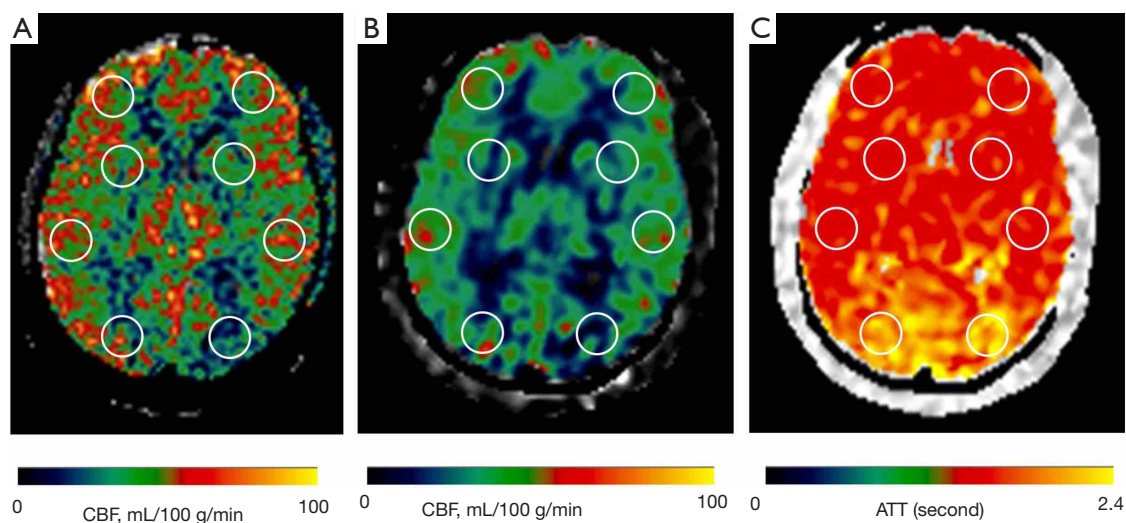


Figure 2 ROIs of bilateral frontal lobes, temporal lobes, occipital lobes, and basal ganglia. (A) PLD =2,025 ms cerebral blood flow map. (B) Transit-corrected cerebral blood flow map. (C) ATT map. ATT, arterial transit time; CBF, cerebral blood flow; ROI, region of interest; PLD, postlabeling delay.

intracranial segment of the bilateral internal carotid arteries (ICAs), the A1 and A2 segments of the bilateral anterior cerebral arteries (ACAs), the M1 and M2 segments of the bilateral middle cerebral arteries (MCAs), the P1 and P2 segments of the bilateral posterior cerebral arteries (PCAs), and the intracranial segments of the bilateral VAs and the basilar artery (BA) were assessed for stenosis. The degree of intracranial artery stenosis was measured according to the method published by the Warfarin-Aspirin Symptomatic

Intracranial Disease (WASID) study (21). The artery with a maximum stenosis rate of $\geq 50\%$ was recorded as a diseased vessel, and the ROI in its blood supply territory is recorded as the lesion ROI. There were several exceptional rules applied, as follows: (I) when the contralateral ACA and the anterior communicating artery are open and supply the normal distal segment of the stenotic proximal ACA, the frontal ROI ipsilateral to the stenotic proximal ACA is presumed to be nonischemic; (II) when the VA stenosis

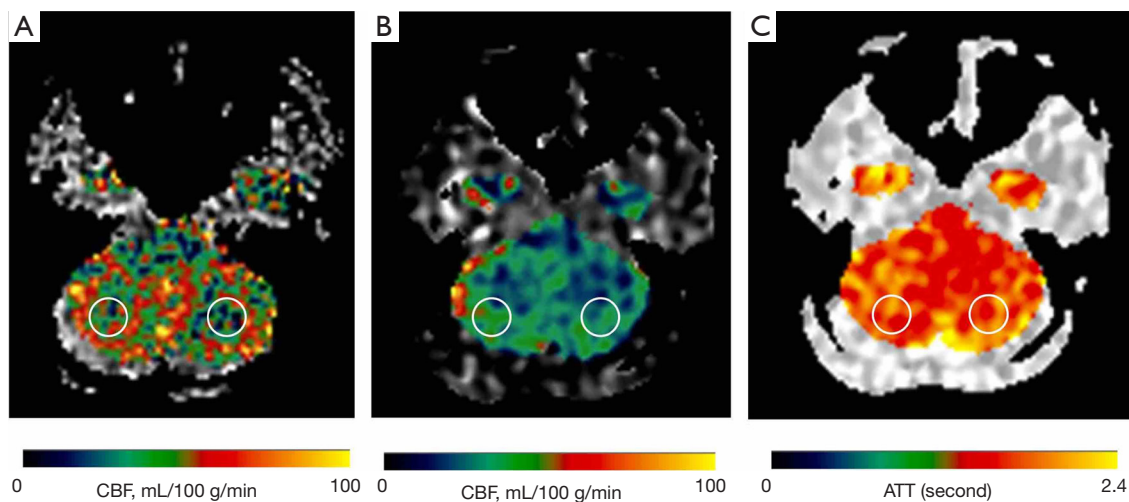


Figure 3 Bilateral cerebellar ROIs. (A) PLD = 2,525 ms cerebral blood flow map. (B) Transit-corrected flow cerebral blood flow map. (C) ATT map. ATT, arterial transit time; CBF, cerebral blood flow; ROI, region of interest; PLD, postlabeling delay.

is unilateral, only the ROI in the ipsilateral cerebellum is recorded as the lesion ROI; and (III) when the posterior communicating artery is open, only the distal segment of the PCA is evaluated for stenosis. ROIs that were in the territories of the stenotic vessels were defined as lesion ROIs, while ROIs other than the lesion ROI were defined as nonischemic ROIs.

Statistical analysis

Statistical analysis was performed using SPSS v. 25.0 (IBM Corp., Armonk, NY, USA) software. A P value <0.05 was considered statistically significant. The continuous variables in this study followed a normal distribution and homogeneity of variance. The intraclass correlation coefficient (ICC) was used for observer consistency testing. Variance analysis was used to compare the differences between the $CBF_{1525\text{ ms}}$, $CBF_{2025\text{ ms}}$, $CBF_{2525\text{ ms}}$, and $CBF_{\text{transit-corrected}}$ groups. A Bland-Altman plot was used to analyze the consistency between the single-PLD-generated CBF and the $CBF_{\text{transit-corrected}}$, and the ICCs were determined. Pearson correlation was performed for the ATT and CBF values, as well as for ATTs between single-PLD-generated CBF and $CBF_{\text{transit-corrected}}$. The differences in CBF values between nonischemic brain ROIs and lesion ROIs were compared using an independent samples *t*-test. Binary logistic regression was applied to analyze the relationship between vascular lesions and the perfusion parameters of the corresponding ROIs. Because of the complex blood supply sources, the CBF values of the

bilateral basal ganglia were not included in the regression analysis.

Results

Evaluation of intracranial artery stenosis

The ICC of intracranial artery stenosis as measured by 2 doctors was 0.978 [95% confidence interval (CI): 0.951–0.990; $P < 0.05$]. Among the 26 patients, 68 ROIs were classified as lesion ROIs due to stenotic or occlusive supplying arteries, including 2 ROIs in the left ACA territory (2.94%), 5 ROIs in the right ACA territory (7.35%), 13 ROIs in the left MCA territory (19.13%), 10 ROIs in the right MCA territory (14.71%), 7 ROIs in the left PCA territory (10.29%), 9 ROIs in the right PCA territory (13.24%), 4 ROIs in the left ICA territory (5.88%), 5 ROIs in the right ICA territory (7.35%), 2 ROIs in the left VA territory (2.94%), 4 ROIs in the right VA territory (5.88%), and 7 ROIs in the BA territory (10.29%) (Figure 4).

Comparison of ASL CBF measurement values between different PLDs

The difference of CBF values at different PLD times was statistically significant ($F = 134.788$; $P < 0.05$; Table 1). The average $CBF_{2525\text{ ms}}$ value was the highest, and the average $CBF_{\text{transit-corrected}}$ value was the lowest. The difference between the CBF of the 2 PLDs was statistically significant ($P < 0.05$).

The Bland-Altman analysis indicated that $CBF_{1525\text{ ms}}$,

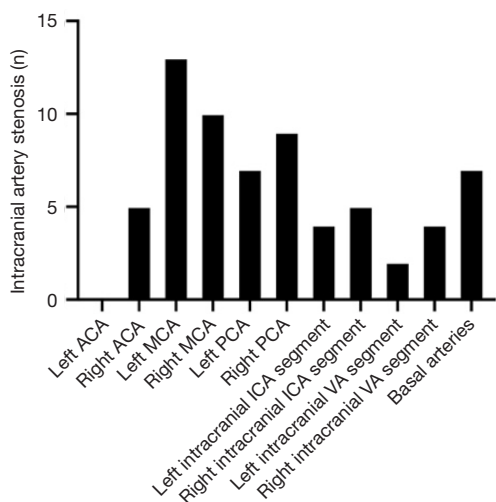


Figure 4 Distribution of the vascular stenosis. ACA, anterior cerebral artery; MCA, middle cerebral artery; PCA, posterior cerebral artery; ICA, internal carotid artery; VA, vertebral artery.

Table 1 CBF measurement values of ASL with different PLDs

Variables	ROI (n)	CBF values (mL/100 g/min)
CBF _{1525 ms}	310	31.36±11.21
CBF _{2025 ms}	310	37.65±9.84
CBF _{2525 ms}	310	41.64±9.05
CBF _{transit-corrected}	310	27.46±8.06

Data are presented as number and mean ± standard deviation. CBF, cerebral blood flow; ASL, arterial spin labeling; PLD, postlabeling delay; ROI, region of interest.

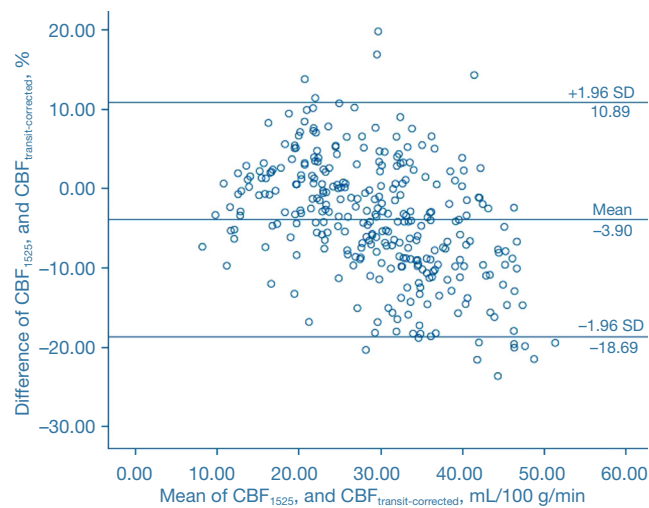


Figure 5 Bland-Altman plot of CBF_{1525 ms} and CBF_{transit-corrected}. CBF, cerebral blood flow; SD, standard deviation.

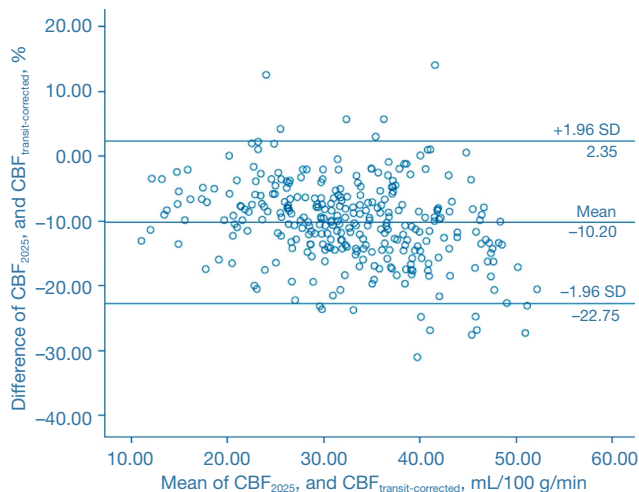


Figure 6 Bland-Altman plot of CBF_{2025 ms} and CBF_{transit-corrected}. CBF, cerebral blood flow; SD, standard deviation.

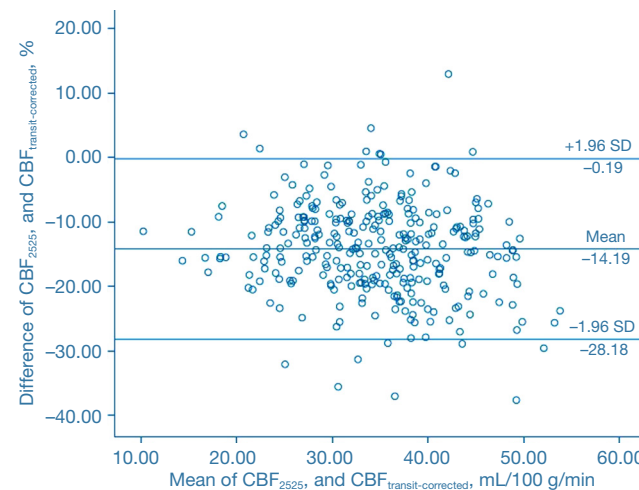


Figure 7 Bland-Altman plot of CBF_{2525 ms} and CBF_{transit-corrected}. CBF, cerebral blood flow; SD, standard deviation.

CBF_{2025 ms} and CBF_{2525 ms} had deviated from CBF_{transit-corrected} to some extent (Figures 5-7). The average difference between the CBF_{transit-corrected} value and the CBF_{1525 ms} value was -3.90%, and the 95% consistency limit was -18.69% to 10.89%. The average difference between the CBF_{transit-corrected} value and the CBF_{2025 ms} value was -10.20%, and the 95% consistency limit was -22.75% to -2.35%. The average difference between the CBF_{transit-corrected} value and the CBF_{2525 ms} value was -14.19%, and the 95% consistency limit was -28.18% to -0.19%. The ICCs were relatively low for the lesion ROIs, as shown in Table 2.

Table 2 Intraclass correlation coefficient of single-PLD 3D pCASL and 7-delay 3D CASL

Variables	ROI		Lesion ROI	
	N	ICC (95% CI)	N	ICC (95% CI)
A	310	0.701 (0.640–0.753)	68	0.360 (0.135–0.550)
B	310	0.747 (0.693–0.792)	68	0.449 (0.237–0.620)
C	310	0.653 (0.584–0.712)	68	0.337 (0.108–0.531)

Values are given as the consistency with 95% CIs in parentheses. A, B, and C indicate the interaction between $CBF_{1525\text{ ms}}$, $CBF_{2025\text{ ms}}$, $CBF_{2525\text{ ms}}$, and $CBF_{\text{transit-corrected}}$, respectively. CI, confidence interval; PLD, postlabeling delay; 3D pCASL, 3-dimensional pseudo-continuous arterial spin labeling; ROI, region of interest; ICC, intraclass correlation coefficient.

Table 3 Correlation between CBF and ATT

Variables	$CBF_{1525\text{ ms}}$	$CBF_{2025\text{ ms}}$	$CBF_{2525\text{ ms}}$	$CBF_{\text{transit-corrected}}$
Correlation coefficients (r)	-0.710	-0.516	-0.224	-0.384
P values	<0.001	<0.001	<0.001	<0.001

The *r* value is the Pearson correlation coefficient. CBF, cerebral blood flow; ATT, arterial transit time.

Table 4 Correlation analysis of the difference between ATT and CBF measurements

Variables	$\Delta CBF_{1525\text{ ms}}$	$\Delta CBF_{2025\text{ ms}}$	$\Delta CBF_{2525\text{ ms}}$
Correlation coefficients (r)	0.645	0.310	-0.150
P values	<0.001	<0.001	0.008

The *r* value is the Pearson correlation coefficient. Δ indicates the difference between the values of $CBF_{1525\text{ ms}}$, $CBF_{2025\text{ ms}}$, $CBF_{2525\text{ ms}}$, and $CBF_{\text{transit-corrected}}$. ATT, arterial transit time; CBF, cerebral blood flow.

Correlation between perfusion and ATT

The CBF values of different PLDs were negatively correlated with the ATT, and the correlation was statistically significant ($P < 0.05$; *Table 3*). The ATT statistically correlated with the difference between CBF generated with single PLD and $CBF_{\text{transit-corrected}}$, with correlation coefficients ranging from 0.645 to -0.150 ($P < 0.05$; *Table 4*).

Analysis of risk factors for moderate, severe, or occlusive vascular lesions

The $CBF_{\text{transit-corrected}}$, $CBF_{1525\text{ ms}}$, $CBF_{2025\text{ ms}}$, and $CBF_{2525\text{ ms}}$ values of the lesion ROIs were significantly lower than the nonischemic ROIs ($t=7.215$, $t=5.245$, $t=6.233$, $t=4.441$, respectively; $P < 0.001$). The ATTs of the lesion ROIs were significantly longer than the nonischemic ROIs (1.92 ± 0.15 vs. 1.80 ± 0.14 s, respectively; *Table 5*). Binary logistic regression showed that ATT and $CBF_{\text{transit-corrected}}$ correlated

with moderate or above-moderate vascular stenosis ($P < 0.05$; *Table 6*).

Discussion

In this study, we used 7-delay 3D-pCASL and single-PLD 3D-pCASL technology to analyze the perfusion status in patients with ICAS and investigated the factors affecting the quantification of CBF in these patients. We found that the $CBF_{\text{transit-corrected}}$ was the lowest, followed by $CBF_{1525\text{ ms}}$ and $CBF_{2025\text{ ms}}$, while the $CBF_{2525\text{ ms}}$ was the highest. There were discrepancies of perfusion parameters between 7-delay 3D-pCASL and single-PLD 3D-pCASL. All CBF measures were related to ATT, but only $CBF_{\text{transit-corrected}}$ and ATT correlated with the presence of moderate to severe vascular stenosis or occlusion.

One of the difficulties regarding the precise estimation of CBF is the modification of the optimal PLD under variable hemodynamic status. The estimation of CBF

Table 5 Comparison of perfusion parameters between nonischemic ROIs and lesion ROIs

CBF parameters (mL/100 g/min)	Nonischemic ROIs	Lesion ROIs	<i>t</i>	P
CBF _{1525 ms}	32.41±10.35	24.28±10.30	5.245	<0.001
CBF _{2025 ms}	39.70±9.48	30.77±9.66	6.233	<0.001
CBF _{2525 ms}	44.20±8.97	38.06±9.66	4.441	<0.001
CBF _{transit-corrected}	30.11±6.55	22.15±8.68	7.215	<0.001
ATT	1.80±0.14	1.92±0.15	-5.780	<0.001

Data are presented as mean ± standard deviation. Independent sample *t*-test. ROI, regions of interest; CBF, cerebral blood flow; ATT, arterial transit time.

Table 6 Analysis of risk factors for moderate and severe vascular stenosis or occlusion

Variables	B	SE	Wald	P	OR	95% CI
CBF _{1525 ms}	0.031	0.031	1.041	0.308	1.032	0.972–1.096
CBF _{2025 ms}	-0.054	0.034	2.466	0.116	0.947	0.886–1.013
CBF _{2525 ms}	0.033	0.027	1.452	0.228	1.033	0.980–1.090
CBF _{transit-corrected}	-0.082	0.036	5.213	0.022	0.921	0.859–0.988
ATT	5.523	1.427	14.986	<0.001	250.436	15.284–4,103.434

CBF, cerebral blood flow; ATT, arterial transit time; B, coefficient value; SE, standard error; OR, odds ratio; CI, confidence interval.

tends to increase with the prolongation of PLD (22). Prolongation of PLD will permit more labeled collateral flow to arrive at the sampling plane, thus resulting in a higher signal measured (23). Although this problem can be partially solved by using 7-delay 3D-pCASL, which samples several PLD points along the ASL uptake and decay curve, the accuracy of CBF quantification is still affected by the number of delays and transit-time correction. For example, in the study by van der Thiel *et al.* (24), CBF estimated from 7-delay 3D-pCASL was found to obtain a higher value for the corrected flow maps than for the uncorrected flow maps; moreover, with multidelay ASL sequences, CBF values were identified to be higher in a higher number of delays than in a lower number of delays. In this study, 7-delay sequences provided a 10% higher estimation of transit time-corrected flow on average across the entire brain than did the 3-delay sequence in healthy people. We adopted the same 7-delay sequence in our study and demonstrated approximate CBF values in the nonischemic ROIs. However, single-PLD ASL led to a significantly higher estimated CBF than did the 7-delay sequence in our study, both in the nonischemic regions and ischemic lesion regions. If the absolute values for CBF are subjected to a comparison, the effect of different compartment modeling

should be noted. This study used the following types of compartment modeling: a single-compartment model for single PLD and a 2-compartment (vascular/tissue) model for 7-delay pCASL. Acquisition of multidelay images can differentiate concomitant contributions of intravascular flow from tissue compartments, while single-PLD ASL may increase the ASL signal in feeding arterial vessels in the case of proximal vessel occlusion (17). Quantitative perfusion estimates based on ASL can be obtained from a number of models. The T1 model is vulnerable to potential systematic errors in ASL. These errors come from variable transit time, exchanges of tagged water between the capillaries and tissue and its effect on the T1 relaxation time, and incomplete tagged water extraction from the capillaries. The general kinetic model, as used for the single-PLD ASL in this study, is presumed to comply with three main assumptions. First, the delay time should be longer than the ATT, so the magnetization-tagged blood is received by the tissue of interest. Second, the bolus is located within the tissue (no outflow condition) because of the large water pool. Third, due to T_{1a} , there is a decrease of magnetization of the labelled blood water. Although the last assumption may not be exactly true, the related error is not typically significant because the difference between the T1 relaxation

of tissue and blood is usually small (25).

Furthermore, previous studies have proposed that the CBF after correction is more stable and repeatable in healthy people (4,26-28). It is of note that the Bland-Altman analysis in our study showed that the CBF values derived from the single PLD deviated from those of the multidelay pCASL. The analysis of ICC demonstrated low consistency between the CBF values of the single-PLD and multi-PLD pCASL, especially in ischemic regions. This suggests that in cases where multi-PLD pCASL is not available, single PLD should be used cautiously under clinical conditions. Haller *et al.* proposed that in patients with known cerebrovascular disease, both long-postlabel delay single-time point ASL and multidelay ASL were helpful in the accurate quantification of CBF. The former will reduce the error caused by slow blood flow not arriving at the tissue bed by the time of imaging, although adequate CBF that arrives later than expected can lead to an overestimation of CBF (17).

In our study, ATT showed a significant correlation with CBF measures for both the corrected and noncorrected measures. When $CBF_{\text{transit-corrected}}$ was taken as the reference value, ATT had a significant impact on the deviation of the CBF values generated with single-PLD ASL, especially those with a relatively short PLD. However, even after correction, CBF may not be sufficiently accurate to reflect the hemodynamic status in severe stenotic vascular disease. In the study of Moyamoya disease by Fan *et al.*, it was found that ATT correction by multidelay acquisitions improved consistency with PET, but CBF remained underestimated in the presence of long transit delays (18). ATT prolongation causes an error in CBF measurement during ASL (5). Ishida *et al.* conducted a simulation and showed that the accuracy of CBF was strongly affected by ATT. They also found that 7-delay ASL significantly underestimated the ATT and subsequently the CBF, which was evident in the distal ACA, MCA, and PCA (29). Although a long labeling duration and a long delay may help to accurately measure the CBF value of the distal end of intracranial large vessels and compensate for the underestimation of CBF caused by a short PLD, there will be a tradeoff of a low signal. A recent study suggested that an ATT-based combination strategy is less ATT dependent and improves CBF measurement accuracy compared with single-delay protocols in severe stenotic diseases (30).

Our results demonstrated increased ATT and reduced CBF in ROIs which were supplied by the stenotic or occlusive arteries. Vascular stenosis leads to slow blood flow and decreased perfusion in the lesion area, while the

existence of peripheral collateral circulation results in a prolonged vascular path. The low-perfusion state of brain tissue leads to significantly prolonged ATT (31). Increased ATT and reduced CBF are potentially the hallmark of brain ischemia. Previous studies have demonstrated that CBF measurements derived from pCASL and dynamic susceptibility contrast were highly and significantly correlated with hypoperfused regions (10,32). According to our observations, ATT is sensitive to ischemia and can be used as a predictive factor. A recent study also proposed that ATT itself might have a potential role in detecting compromised hemodynamic states (33). It is worth noting that CBF derived from a single-PLD ASL was not predictive of brain ischemia in our study. Only $CBF_{\text{transit-corrected}}$ was consistent with the presence of ischemic territories. In a recent study using perfusion single-photon emission computerized tomography (SPECT) results as the standard, multiple-PLD-derived CBF achieved a 100% sensitivity and 100% negative predictive value for the detection of hypoperfusion, which was significantly better than the sensitivity (95% CI: 44–80%) and negative predictive value (95% CI: 88–97%) of the standard PLD-derived CBF (34).

There were several limitations to this study. First, the scanning parameters for single-PLD and multi-PLD pCASL were not exactly the same in this study. The spatial resolution of single-PLD pCASL was higher than that of multi-PLD pCASL, and a greater number of excitations were used to maintain the signal-to-noise ratio (SNR). However, multi-PLD pCASL cannot be performed in the same way because of the long scanning time. Although there were differences in the spatial resolution and SNR, their effects on the measurement of CBF may be insignificant since the ROIs in this study were large enough to eliminate the effects. Second, due to the lack of a gold standard, the ischemic area could not be accurately identified in our patients. We defined the ROIs supplied by arteries with a stenosis degree of more than 50% as the ischemic regions; however, due to the existence of collateral circulation, some regions might not have been truly ischemic. However, detecting these regions is still useful because they are vulnerable to an attack. Third, tandem lesions on some of the vascular pathways in some patients might have exerted a superimposition effect, which could have led to an underestimation of vascular disease when evaluating the largest stenosis only. Lastly, the watershed area which is important in ischemic cerebrovascular disease was not evaluated in this study and needs to be further investigated.

Conclusions

Our results indicated discrepancies in the quantification of CBF between single-PLD ASL and multidelay ASL, which may be misleading in clinical applications. The difference in the estimation of CBF in patients with ICAS is multifactorial and includes technical issues and hemodynamical factors. CBF measures were all dependent on ATT. The perfusion parameters generated using standard single-PLD ASL were more affected by ATT compared with multidelay ASL. ATT was demonstrated to be predictive of stenotic vascular territories, which is useful in the evaluation of brain ischemia in intracranial atherosclerotic disease.

Acknowledgments

The authors thank Dr. Xiaocheng Wei from GE Healthcare for help in solving Enhanced ASL technical problems.

Funding: None.

Footnote

Conflicts of Interest: All authors have completed the ICMJE uniform disclosure form (available at <https://qims.amegroups.com/article/view/10.21037/qims-22-969/coif>). The authors have no conflicts of interest to declare.

Ethical Statement: The authors are accountable for all aspects of the work in ensuring that questions related to the accuracy or integrity of any part of the work are appropriately investigated and resolved. The study was conducted in accordance with the Declaration of Helsinki (as revised in 2013). The study protocol was approved by the Institutional Review Board of the China-Japan Friendship Hospital (No. 2015-23). Informed consent was obtained from each participant.

Open Access Statement: This is an Open Access article distributed in accordance with the Creative Commons Attribution-NonCommercial-NoDerivs 4.0 International License (CC BY-NC-ND 4.0), which permits the non-commercial replication and distribution of the article with the strict proviso that no changes or edits are made and the original work is properly cited (including links to both the formal publication through the relevant DOI and the license). See: <https://creativecommons.org/licenses/by-nc-nd/4.0/>.

References

1. Wang Y, Zhao X, Liu L, Soo YO, Pu Y, Pan Y, Wang Y, Zou X, Leung TW, Cai Y, Bai Q, Wu Y, Wang C, Pan X, Luo B, Wong KS; . Prevalence and outcomes of symptomatic intracranial large artery stenoses and occlusions in China: the Chinese Intracranial Atherosclerosis (CICAS) Study. *Stroke* 2014;45:663-9.
2. Pohmann R, Budde J, Auerbach EJ, Adriany G, Uğurbil K. Theoretical and experimental evaluation of continuous arterial spin labeling techniques. *Magn Reson Med* 2010;63:438-46.
3. Murphy K, Harris AD, Diukova A, Evans CJ, Lythgoe DJ, Zelaya F, Wise RG. Pulsed arterial spin labeling perfusion imaging at 3 T: estimating the number of subjects required in common designs of clinical trials. *Magn Reson Imaging* 2011;29:1382-9.
4. Neumann K, Schidlowski M, Günther M, Stöcker T, Düzel E. Reliability and Reproducibility of Hadamard Encoded Pseudo-Continuous Arterial Spin Labeling in Healthy Elderly. *Front Neurosci* 2021;15:711898.
5. Alsop DC, Detre JA, Golay X, Günther M, Hendrikse J, Hernandez-Garcia L, Lu H, MacIntosh BJ, Parkes LM, Smits M, van Osch MJ, Wang DJ, Wong EC, Zaharchuk G. Recommended implementation of arterial spin-labeled perfusion MRI for clinical applications: A consensus of the ISMRM perfusion study group and the European consortium for ASL in dementia. *Magn Reson Med* 2015;73:102-16.
6. Zhuang C, Poubanc J, Mcketton L, Venkatraghavan L, Sobczyk O, Duffin J, Crawley AP, Fisher JA, Wu R, Mikulis DJ. The value of a shorter-delay arterial spin labeling protocol for detecting cerebrovascular impairment. *Quant Imaging Med Surg* 2021;11:608-19.
7. Martin SZ, Madai VI, von Samson-Himmelstjerna FC, Mutke MA, Bauer M, Herzig CX, Hetzer S, Günther M, Sobesky J. 3D GRASE pulsed arterial spin labeling at multiple inflow times in patients with long arterial transit times: comparison with dynamic susceptibility-weighted contrast-enhanced MRI at 3 Tesla. *J Cereb Blood Flow Metab* 2015;35:392-401.
8. Yu H, Li Y, Feng Y, Zhang L, Yao Z, Liu Z, Gao W, Chen Y, Xie S. Enhanced Arterial Spin Labeling Magnetic Resonance Imaging of Cerebral Blood Flow of the Anterior and Posterior Circulations in Patients With Intracranial Atherosclerotic Stenosis. *Front Neurosci* 2022;15:823876.

9. Kim HG, Lee JH, Choi JW, Han M, Gho SM, Moon Y. Multidelay Arterial Spin-Labeling MRI in Neonates and Infants: Cerebral Perfusion Changes during Brain Maturation. *AJNR Am J Neuroradiol* 2018;39:1912-8.
10. Wang DJ, Alger JR, Qiao JX, Gunther M, Pope WB, Saver JL, Salamon N, Liebeskind DS; . Multi-delay multi-parametric arterial spin-labeled perfusion MRI in acute ischemic stroke - Comparison with dynamic susceptibility contrast enhanced perfusion imaging. *Neuroimage Clin* 2013;3:1-7.
11. Xu Y, Lü JH, Ma L, Chen WJ, Lou X. Quantitative Measurement of Cerebral Blood Flow in Enhanced Pseudo-continuous Arterial Spin Labeling Perfusion Imaging in Patients with Intracranial Atherosclerotic Stenosis. *Zhongguo Yi Xue Ke Xue Yuan Xue Bao* 2016;38:679-85.
12. Xu X, Tan Z, Fan M, Ma M, Fang W, Liang J, Xiao Z, Shi C, Luo L. Comparative Study of Multi-Delay Pseudo-Continuous Arterial Spin Labeling Perfusion MRI and CT Perfusion in Ischemic Stroke Disease. *Front Neuroinform* 2021;15:719719.
13. Wang R, Yu S, Alger JR, Zuo Z, Chen J, Wang R, An J, Wang B, Zhao J, Xue R, Wang DJ. Multi-delay arterial spin labeling perfusion MRI in moyamoya disease--comparison with CT perfusion imaging. *Eur Radiol* 2014;24:1135-44.
14. Fan AP, Khalighi MM, Guo J, Ishii Y, Rosenberg J, Wardak M, Park JH, Shen B, Holley D, Gandhi H, Haywood T, Singh P, Steinberg GK, Chin FT, Zaharchuk G. Identifying Hypoperfusion in Moyamoya Disease With Arterial Spin Labeling and an (15)O-Water Positron Emission Tomography/Magnetic Resonance Imaging Normative Database. *Stroke* 2019;50:373-80.
15. Hu Y, Liu R, Gao F. Arterial Spin Labeling Magnetic Resonance Imaging in Healthy Adults: Mathematical Model Fitting to Assess Age-Related Perfusion Pattern. *Korean J Radiol* 2021;22:1194-202.
16. Han H, Ning Z, Yang D, Yu M, Qiao H, Chen S, Chen Z, Li D, Zhang R, Liu G, Zhao X. Associations between cerebral blood flow and progression of white matter hyperintensity in community-dwelling adults: a longitudinal cohort study. *Quant Imaging Med Surg* 2022;12:4151-65.
17. Haller S, Zaharchuk G, Thomas DL, Lovblad KO, Barkhof F, Golay X. Arterial Spin Labeling Perfusion of the Brain: Emerging Clinical Applications. *Radiology* 2016;281:337-56.
18. Fan AP, Guo J, Khalighi MM, Gulaka PK, Shen B, Park JH, Gandhi H, Holley D, Rutledge O, Singh P, Haywood T, Steinberg GK, Chin FT, Zaharchuk G. Long-Delay Arterial Spin Labeling Provides More Accurate Cerebral Blood Flow Measurements in Moyamoya Patients: A Simultaneous Positron Emission Tomography/MRI Study. *Stroke* 2017;48:2441-9.
19. Wu B, Lou X, Wu X, Ma L. Intra- and interscanner reliability and reproducibility of 3D whole-brain pseudo-continuous arterial spin-labeling MR perfusion at 3T. *J Magn Reson Imaging* 2014;39:402-9.
20. Dai W, Robson PM, Shankaranarayanan A, Alsop DC. Reduced resolution transit delay prescan for quantitative continuous arterial spin labeling perfusion imaging. *Magn Reson Med* 2012;67:1252-65.
21. Samuels OB, Joseph GJ, Lynn MJ, Smith HA, Chimowitz MI. A standardized method for measuring intracranial arterial stenosis. *AJNR Am J Neuroradiol* 2000;21:643-6.
22. Dai W, Fong T, Jones RN, Marcantonio E, Schmitt E, Inouye SK, Alsop DC. Effects of arterial transit delay on cerebral blood flow quantification using arterial spin labeling in an elderly cohort. *J Magn Reson Imaging* 2017;45:472-81.
23. Lyu J, Ma N, Liebeskind DS, Wang DJ, Ma L, Xu Y, Wang T, Miao Z, Lou X. Arterial Spin Labeling Magnetic Resonance Imaging Estimation of Antegrade and Collateral Flow in Unilateral Middle Cerebral Artery Stenosis. *Stroke* 2016;47:428-33.
24. van der Thiel M, Rodriguez C, Giannakopoulos P, Burke MX, Lebel RM, Gninenko N, Van De Ville D, Haller S. Brain Perfusion Measurements Using Multidelay Arterial Spin-Labeling Are Systematically Biased by the Number of Delays. *AJNR Am J Neuroradiol* 2018;39:1432-8.
25. Alsaedi A, Thomas D, Bisdas S, Golay X. Overview and Critical Appraisal of Arterial Spin Labelling Technique in Brain Perfusion Imaging. *Contrast Media Mol Imaging* 2018;2018:5360375.
26. Cohen AD, Agarwal M, Jagra AS, Nencka AS, Meier TB, Lebel RM, McCrea MA, Wang Y. Longitudinal Reproducibility of MR Perfusion Using 3D Pseudocontinuous Arterial Spin Labeling With Hadamard-Encoded Multiple Postlabeling Delays. *J Magn Reson Imaging* 2020;51:1846-53.
27. Parkes LM, Rashid W, Chard DT, Tofts PS. Normal cerebral perfusion measurements using arterial spin labeling: reproducibility, stability, and age and gender effects. *Magn Reson Med* 2004;51:736-43.
28. Pfefferbaum A, Chanraud S, Pitel AL, Shankaranarayanan A, Alsop DC, Rohlfing T, Sullivan EV. Volumetric cerebral perfusion imaging in healthy adults: regional distribution,

- laterality, and repeatability of pulsed continuous arterial spin labeling (PCASL). *Psychiatry Res* 2010;182:266-73.
29. Ishida S, Kimura H, Isozaki M, Takei N, Fujiwara Y, Kanamoto M, Kosaka N, Matsuda T, Kidoya E. Robust arterial transit time and cerebral blood flow estimation using combined acquisition of Hadamard-encoded multi-delay and long-labeled long-delay pseudo-continuous arterial spin labeling: a simulation and in vivo study. *NMR Biomed* 2020;33:e4319.
 30. Amemiya S, Watanabe Y, Takei N, Ueyama T, Miyawaki S, Koizumi S, Kato S, Takao H, Abe O, Saito N. Arterial Transit Time-Based Multidelay Combination Strategy Improves Arterial Spin Labeling Cerebral Blood Flow Measurement Accuracy in Severe Steno-Occlusive Diseases. *J Magn Reson Imaging* 2022;55:178-87.
 31. Yun TJ, Sohn CH, Han MH, Kang HS, Kim JE, Yoon BW, Paeng JC, Choi SH, Kim JH, Song IC, Chang KH. Effect of delayed transit time on arterial spin labeling: correlation with dynamic susceptibility contrast perfusion magnetic resonance in moyamoya disease. *Invest Radiol* 2013;48:795-802.
 32. Wang DJ, Alger JR, Qiao JX, Hao Q, Hou S, Fiaz R, Gunther M, Pope WB, Saver JL, Salamon N, Liebeskind DS; . The value of arterial spin-labeled perfusion imaging in acute ischemic stroke: comparison with dynamic susceptibility contrast-enhanced MRI. *Stroke* 2012;43:1018-24.
 33. Takeuchi K, Isozaki M, Higashino Y, Kosaka N, Kikuta KI, Ishida S, Kanamoto M, Takei N, Okazawa H, Kimura H. The Utility of Arterial Transit Time Measurement for Evaluating the Hemodynamic Perfusion State of Patients with Chronic Cerebrovascular Stenosis or Occlusive Disease: Correlative Study between MR Imaging and (15) O-labeled H(2)O Positron Emission Tomography. *Magn Reson Med Sci* 2022. [Epub ahead of print]. doi: 10.2463/mrms.mp.2020-0123.
 34. Setta K, Matsuda T, Sasaki M, Chiba T, Fujiwara S, Kobayashi M, Yoshida K, Kubo Y, Suzuki M, Yoshioka K, Ogasawara K. Diagnostic Accuracy of Screening Arterial Spin-Labeling MRI Using Hadamard Encoding for the Detection of Reduced CBF in Adult Patients with Ischemic Moyamoya Disease. *AJNR Am J Neuroradiol* 2021;42:1403-9.

Cite this article as: Yu H, Ouyang Y, Feng Y, Sun S, Zhang L, Liu Z, Tian H, Xie S. Comparison of single-postlabeling delay and seven-delay three-dimensional pseudo-continuous arterial spin labeling in the assessment of intracranial atherosclerotic disease. *Quant Imaging Med Surg* 2023;13(4):2514-2525. doi: 10.21037/qims-22-969